Evaluation on the axial compression mechanical properties of short BFRP laminated bamboo lumber columns

Wenjing Zhou [1,2], Haitao Li[1,2*], Sarah Mohrmann [1,2], Hang Li[1,2], Zhenhua Xiong[3], Rodolfo Lorenzo[4]

[1] College of Civil Engineering, Nanjing Forestry University, Nanjing 210037, China;

[2] Joint International Research Laboratory for Bio-composite Building Materials and Structures, Nanjing Forestry University, Nanjing 210037, China

[3] Ganzhou Sentai bamboo company LTD, Ganzhou 341001, China.

[4] University College London, London WC1E 6BT, UK.

*Corresponding author: Haitao Li, Professor, E-mail: lhaitao1982@126.com

Abstract: To investigate the effect of BFRP (basalt fiber) reinforced short laminated bamboo lumber (LBL) columns on axial compressive static performance, axial compression tests of twelve BFRP reinforced short LBL columns and three normal short LBL columns were conducted, and tensile tests of 13 BFRP were carried out. The test results show that the failure mode of BFRP reinforced short LBL columns was consistent with that of normal short LBL columns, buckling failure and adhesive layer failure. With the increase of BFRP cloth ratio, the bearing capacity of the columns increased. However, when the cloth ratio exceeded 2.3% (4 layers of BFRP), the average improvement of the load-bearing capacity was not obvious, and the reasonable cloth ratio was reached at 2.3%. The short LBL columns wrapped BFRP showed good compressive ductility, and the higher the cloth ratio of BFRP, the better the compressive ductility. Based on the suitable analysis of test data and referring to the relevant methods of fiber reinforced wood columns, the calculation model of axial compressive bearing capacity and stress-strain relationship model of BFRP reinforced short LBL columns were established. The comparison between theoretical calculation and experimental results verified the reliability and accuracy of the proposed bearing capacity calculation model and stress-strain model.

Keywords: Laminated bamboo lumber; BFRP; Axial compression; Bearing capacity; Stress-strain relationship

1 Introduction

The social demand for green and sustainable building materials is steadily increasing, while the quantity of industrial wood is very scarce, and the gap between supply and demand of wood is becoming increasingly prominent. Bamboo has a short growth cycle, abundant resources, large cultivation area and accumulation [1]. It is a renewable resource and deserves to be an ecological material in the new era. Especially in the case of wood shortage, sustainable and green bamboo is undoubtedly a good choice to replace wood. Therefore, it is very important to study the structure of bamboo.

The bamboo canes have a variable cross-section and material properties over the length [2] and the hollow cross-section requires difficult joints. This makes it difficult to meet the requirements of modern bamboo buildings for component mechanical properties and spatial structure [3]. Advances in production technology have made it possible to produce engineered bamboo products [4]. Engineered bamboo products overcome the shortcomings of original bamboo, retain the advantages of original bamboo, and are becoming increasingly popular [5-9]. Laminated bamboo lumber (LBL) is a common kind of engineered bamboo products [10-11]. What is LBL? LBL is a bamboo board composed of many basic bamboo units through certain manufacturing processes. The basic processes include carbonization, drying, gluing, blank assembly, hot pressing, gluing, etc. [12].

Researchers paid much attention to the production process [12-16] and mechanical

properties [17-28] of LBL. Li et al [29-32] found that the production process of LBL can flexibly control the size and length of its components, and its mechanical properties are good, such as high elastic modulus, compressive strength along grain and tensile strength along the grain. LBL can partly replace wood as building materials, and can also be used as components of bamboo (wood) structures [33], which offers a good application prospect [34]. However, as a vertical structural element, LBL columns are susceptible to rot, moth-eaten, warpage and dry shrinkage cracking during its service life. Their damage is further accelerated under harsh environmental conditions, leading to a reduction in strength and stiffness, thus endangering the safety of the entire structure.

Composites are increasingly used in construction [35-36], especially fiber reinforced polymer (FRP) [37-38], because of their good strength-to-weight ratio, high corrosion resistance and ease of cutting. An important application of FRP composites is the reinforcement of brittle materials [39] such as concrete, timber, engineering bamboo [40-42]. Making full use of the advantages of FRP can not only improve the problems associated with components in the service life, such as pest [43], corrosion [44], fire [45], but also reinforce the existing components and improve their bearing capacity [46]. Basalt fiber reinforced polymer (BFRP), as a new type of composite material, is another high-tech fiber composite material after carbon fibers [47]. BFRP has an interesting relationship between quality and cost compared with the conventional FRPs [48]. BFRP is much cheaper than carbon fibre (CFRP), and its price is only one eighth to one sixth of that of CFRP [49] and has higher mechanical properties (tensile strength and elastic modulus) than glass fiber reinforced plastics (GFRP) [50]. Basalt fiber can be used as a potential candidate for carbon fiber reinforced materials to achieve the same mechanical properties as carbon fiber reinforced materials [47]. Additionally, it has a wide range of raw materials, an environmentally friendly production process and meets the requirements of green sustainable development [51-52].

FRP is also widely used to reinforced timber columns [53-57]. FRP has different reinforcement effects on timber columns with different cross-sectional shapes [58], the reinforcement effect of circular is better than that of square timber columns [59-60]. Qiao [57] carried out axial compression experiments on CFRP reinforced square timber filled steel tube stub columns, and CFRP can increase the axial compressive strength of columns. Emerson [61] studied the bearing capacity of bare timber columns and rotten timber pier columns with GFRP, showing that the bearing capacity of the GFRP reinforced timber columns was about 17% higher than the bare timber columns. Chidiaq [62] carried out axial compression experiments on CFRP reinforced intact timber columns, showing that the bearing capacity of the timber columns with CFRP increased by 15%-25%.

Few studies evaluated FRP reinforced short LBL columns. Hong [63], Wang [64] and Li [65] carried out axial compression experiments on FRP reinforced short LBL columns, studied the ultimate strength of FRP reinforced short LBL columns, but did not propose a universal model of stress-strain model. Herein, the effect of BFRP on the axial compressive performance of BFRP reinforced short LBL columns was investigated. Twelve axial compression tests of BFRP reinforced short LBL columns and three normal short LBL columns were completed. Based on the test results, the load-displacement

curves and stress-strain curves were analyzed, the changes of ductility and load-bearing capacity were evaluated. A calculation model of bearing capacity was established, and a universal model of stress-strain model was proposed, which can describe both the stress-strain relationship of short LBL columns without BFRP and with BFRP.

2. Materials and test methods

2.1 Materials and specimens

The raw material of LBL is Phyllostachys edulis from the surrounding areas of Yong'an City, Fujian Province. Its growth cycle is short, the rod shape is thick and straight, and it is suitable for construction. The specimens were processed by Jiangxi Ganzhou Sentai bamboo and Wood Co., Ltd. The LBL specimens were made of 2005 mm×21 mm×7 mm bamboo strips prepared by hot pressing for 15min with resorcinol as adhesive under the conditions of main pressure of 9 MPa, lateral pressure of 6.5 MPa and a temperature of 157 ℃. The manufacturing process of LBL is shown in **Fig. 1**.

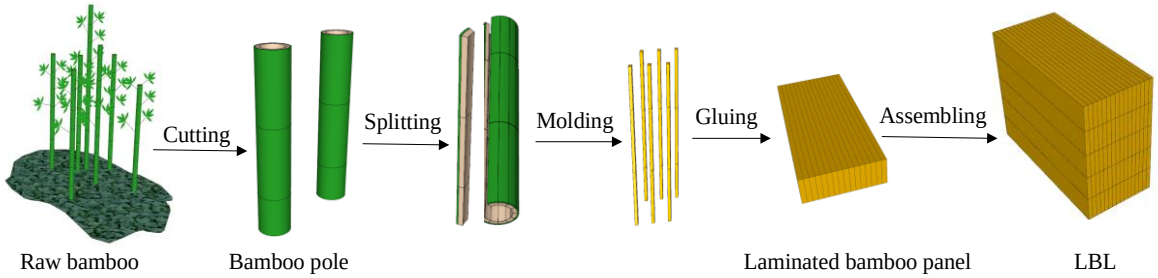

Fig. 1 Schematic diagram of LBL production

The BFRP cloth was wrapped on the short LBL columns manually and the process is as follows: First the BFRP cloth was cut and trimmed to required size according to the geometry of the columns; Second the adhesive (phenolic resin) was applied evenly on the clean-and-dry surface of columns and BFRP cloth, then the BFRP cloth was wrapped on the columns; Third the BFRP-wrapped columns were covered with plastic films, the tests shall not be conducted until the adhesive was completely cured within 30 days.

The cross-section of the short LBL column designed for the test is shown in **Fig. 2** . The cross-section was 100 mm×100 mm with four chamfers of 10 mm. The height of the short LBL column was 300 mm. There are 15 columns, three in each group, including 12 short LBL columns with BFRP (the cloth ratio was 1.2%, 1.8%, 2.3% and 2.9% respectively) and 3 short LBL columns without BFRP. The specimen's number shall follow the naming rules below: the normal short LBL columns are expressed by SA300 and the BFRP reinforced short LBL columns are SnB300, *n* represents the number of layers of BFRP.

The quantity of BFRP can be expressed by the cloth ratio. The cloth ratio is defined as the percentage of the ratio between the BFRP area and the cross-section of BFRP reinforced short LBL columns, calculated with the formula (1):

$$\rho_F = \frac{A_F}{A_a} \times 100\% \quad (1)$$

$$A_F = \left[4 \times (b - 2d) + 4 \times \sqrt{2} d \right] \times t_f \quad (2)$$

$$A_a = b^2 - 2d^2 \quad (3)$$

Where, ρ_F is the cloth ratio; A_F is the area of BFRP; A_a is the cross-sectional area of LBL column; t_f is the wrapping thickness of BFRP; d is chamfers side length; b is the side length of the cross-section.

The number and grouping of the specimens are listed in **Table 1**.

Table 1 Main parameters of specimens

Specimens	A/mm^2	H/mm	d/mm	E_{frp}/GPa	t_f/mm	n	ρ_F %	Number
SA300	100×100	300	10	--	0	0	0	3
S2B300	100×100	300	10	59.5	0.151	2	1.2	3
S3B300	100×100	300	10	59.5	0.151	3	1.8	3
S4B300	100×100	300	10	59.5	0.151	4	2.3	3
S5B300	100×100	300	10	59.5	0.151	5	2.9	3

Note: A is Sectional area; H is column height; d is chamfers side length; E_{frp} is the elastic modulus of BFRP; t_f is the thickness of BFRP; n represents the number of layers of BFRP.

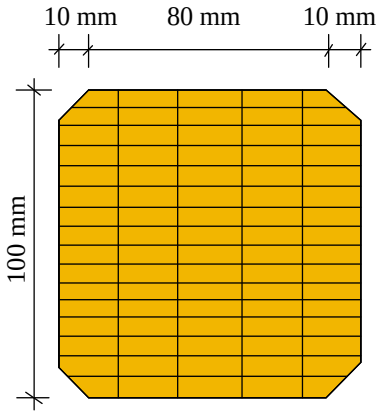

Fig. 2 Cross-section

2.2 Test setup

The test was completed in Jiangning test center of Nanjing Forestry University. The instruments used in the test mainly include microcomputer-controlled electro-hydraulic servo universal testing machine and a TDS-530 data acquisition system. Loading diagram of short columns is shown in **Fig. 3**. During the test, the vertical upward movement of the base loads the test specimens axially. The installation of the displacement meter was fixed by the magnetic meter base and placed vertically to measure the vertical displacement of the upward movement of the instrument base. The test loading was divided into three stages, the first two stages were force control, and the last stage was displacement control. Firstly, the force was increased to 2 kN at a loading ratio of 200 N/s; secondly, the force was increased to 500 kN at a loading ratio of 1.5 kN/s; thirdly, the displacement was controlled and increased to 50mm at a loading ratio of 8 mm /min.

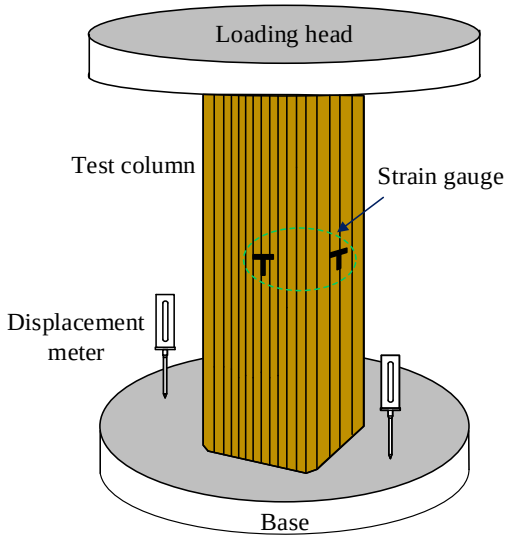

Fig. 3 Loading diagram of short columns

2.3 BFRP Tensile test

The tensile tests of 13 BFRP specimens were carried out, and the tensile performance parameters of BFRP were obtained. The BFRP tensile test specimens were designed into dumbbell shape, so that the failure of the test specimens occurs in the middle. The specific dimension is shown in **Fig. 4.**

The stress-strain curves of BFRP are shown in **Fig. 5**. The average values of BFRP tensile strength and elastic modulus are 1488 MPa and 59.5 GPa respectively, the average peak strain of BFRP is 0.024.

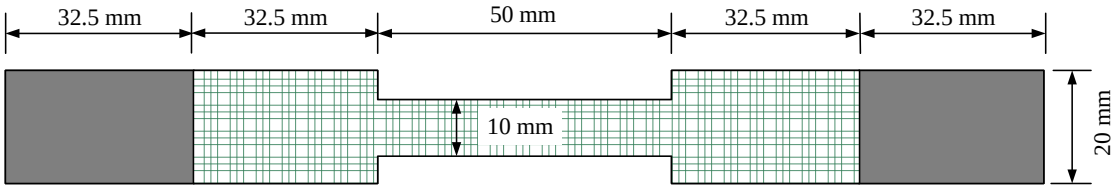

Fig. 4 FRP tensile specimen. All dimensions are in mm

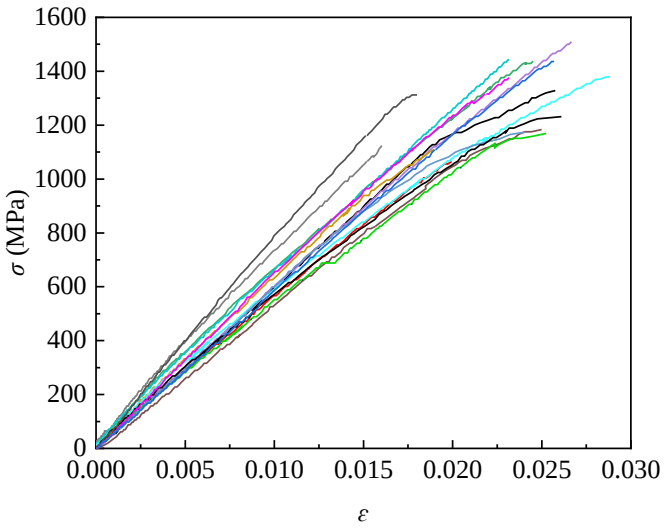

Fig. 5 Stress-strain curves of BFRP

3 Test results and analysis

The main test results are listed in **Table 2**.

Table 2 The main test results

Specimens	P /kN	σ_u /MPa	ρ_F %	Δ_p /mm	Δ_y /mm	u_Δ	E_{cc} /MPa	ε_y	ε_p
SA300-1	536.1	54.7	0	32.4	3.7	8.8	9220	0.0041	0.0146
SA300-2	573.3	58.5	0	31.8	3.7	8.6	9363	0.0039	0.0139
SA300-3	563.8	57.5	0	29.4	3.5	8.4	9190	0.0046	0.0144
Mean value	557.7	56.9	0	31.2	3.6	8.6	9258	0.0042	0.0143
S2B300-1	601.5	60.3	1.2	35.6	3.6	9.9	10938	0.0041	0.0141
S2B300-2	586.9	58.7	1.2	31.7	3.5	9.1	9710	0.0038	0.0146
S2B300-3	543.7	57.5	1.2	34.2	3.5	9.8	9958	0.0037	0.0152
Mean value	577.4	58.8	1.2	33.8	3.5	9.6	10202	0.0039	0.0146
S3B300-1	627.8	64.1	1.8	39.9	4.1	9.7	11014	0.0039	0.0154
S3B300-2	590.6	60.3	1.8	34.5	3.3	10.5	9703	0.0034	0.0166
S3B300-3	597.8	61.0	1.8	35.8	3.4	10.5	11148	0.0038	0.0141
Mean value	605.4	61.8	1.8	36.7	3.6	10.2	10621	0.0037	0.0154
S4B300-1	652.3	65.6	2.3	37.5	3.5	10.7	11732	0.0037	0.0177
S4B300-2	618.4	61.9	2.3	35.3	3.4	10.4	11660	0.0034	0.0165
S4B300-3	668.1	67.2	2.3	39.6	4.0	9.9	9998	0.0034	0.0170
Mean value	646.3	64.9	2.3	37.5	3.6	10.3	11130	0.0035	0.0171
S5B300-1	671.4	68.3	2.9	38.5	3.8	10.1	11288	0.0040	0.0176
S5B300-2	640.6	65.1	2.9	39.6	3.7	10.7	13202	0.0028	0.0170
S5B300-3	647.7	66.4	2.9	38.1	3.7	10.3	11580	0.0033	0.0179
Mean value	653.2	66.6	2.9	38.7	3.7	10.4	12023	0.0034	0.0175

Note: P is the ultimate load; σ_u is the ultimate strength; ρ_F is cloth ratio of BFRP; Δ_p is the displacement when the peak load decreases to 85%P_u; Δ_y is the displacement at yield point; u_Δ is the ductility coefficient; E is the elastic modulus ε_y is the yield strain; ε_p is the plastic strain.

3.1 Failure phenomenon

During the process from the initial loading to 70% of ultimate load, there were no obvious cracks and deformation on the surface of the normal short LBL columns. As the load increased to about 95% of ultimate load, the normal short LBL columns were gradually compressed and bulged outward. When the test load reached ultimate load, the bamboo fiber cracked. With the increase of deformation, the cracks grew rapidly and expanded along the axis, the specimens were completely destroyed.

During the initial loading to 95% of ultimate load, failure phenomenon in the BFRP reinforced short LBL columns was similar to the normal short LBL columns. When the load reached ultimate load, the failure of BFRP started at the chamfers and developed inward for all specimens. With the increase of deformation, the fracture of bamboo fiber and BFRP intensified. Until the BFRP broke, the specimens were completely destroyed.

According to the test process, the failure phenomena of all columns can be divided into two types, namely buckling failure and adhesive layer failure, as shown in **Fig. 6**.

(1) Buckling failure. The specific performance was the collapse (**Fig. 6 (a)**) or local buckling of the end (**Fig. 6 (b)**) of the specimens. Due to the different elastic modulus and Poisson's ratio between LBL and base plate, the deformation of LBL and base plate could not be coordinated, and the transverse deformation of the base plate was obviously less than that of LBL. The base plate limited the transverse deformation of the specimens due to friction on the contact surface. The friction had little effect on the transverse deformation in the middle of the specimens height, so the specimens would collapse in the local area of the end.

(2) Adhesive layer failure. The specific performance was the cracking of the cemented joint of LBL (**Fig. 6 (c)**) or the cracking of the joint of BFRP cloth (**Fig. 6 (d)**).

(a) **(b)** **(c)** **(d)**

Fig. 6 Failure phenomena of columns

3.2 Load-displacement curves

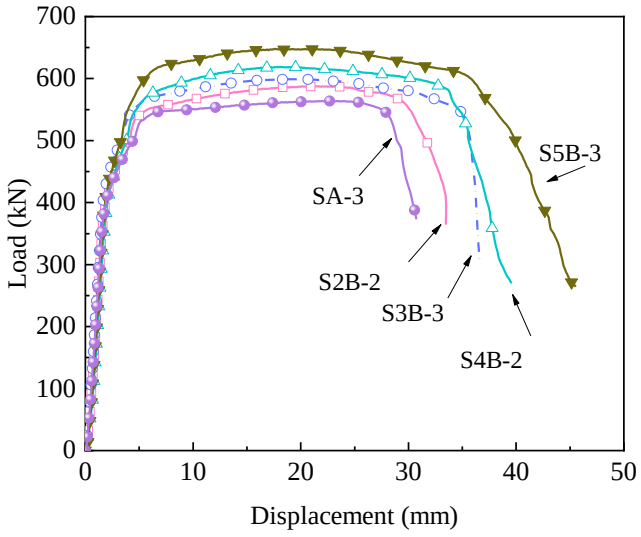

Fig. 7 Load - displacement curve of specimens

Fig. 7 shows the load-displacement curves of specimens. In the initial phase of loading, the applied load was small, the displacement increased linearly with the increasing load. When the load reached about yield point, the stiffness of each group of specimens suddenly decreased, the ability of the specimens to resist deformation

decreased, and the axial displacement continued to increase rapidly, but the load slowly increased. Then the specimens developed the plastic stage, and the axial displacement of the specimens increased rapidly, but the load kept unchanged. When the displacement increased to about ultimate displacement, the load gradually decreased until the specimens were damaged. As the cloth ratio of BFRP increased, the area, enclosed by the load-displacement curve and the coordinate axis, became larger, indicating that the more energy was required for specimen failure.

3.3 Stress-strain curves

Fig. 8 shows the stress-strain curves of specimens. The trends of the stress-strain of the BFRP reinforced short LBL columns were similar to that of the normal short LBL columns. Compared with normal short LBL columns, the lateral strain of BFRP reinforced short LBL columns changed slightly, which showed that LBL did not produce large lateral deformation and that BFRP had a good restraining effect on LBL.

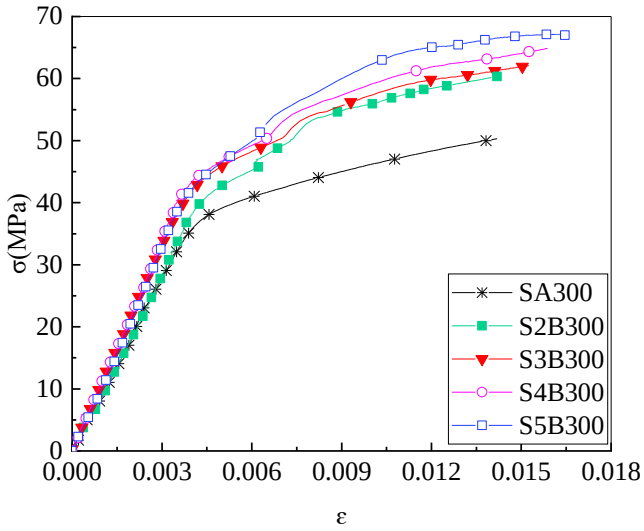

Fig. 8 Stress-strain curves of test specimens

The obvious difference of stress-strain relationship between BFRP reinforced short LBL column and normal short LBL columns was mainly reflected in the elastic-plastic stage. The larger the cloth ratio of BFRP was, the fuller the elastic-plastic stage was. The average peak stresses of specimens were 56.9 MPa, 58.8 MPa, 61.8 MPa, 64.9 MPa and 68.1 MPa, respectively. Compared with the normal short LBL columns, the peak stresses increased by 2.8%, 8.6%, 14.1% and 19.7%, respectively. This showed that the BFRP cloth has an effective restraining function and improves the load-bearing capacity of specimens.

3.4 Ductility

The ductility coefficient [66] is used to calculate the plastic deformation capacity of the specimens, the formula is as follows:

$$u_{\Delta} = \frac{\Delta_{p}}{\Delta_{y}} \tag{4}$$

Where Δ_p is the displacement when the peak load decreases to 85%P_u; Δ_y is the displacement at yield point; Δ_p and Δ_y are determined by the load- displacement curves.

Fig. 9 shows the relationship between cloth ratio and ductility coefficient. BFRP can improve specimens ductility .The greater the cloth ratio of BFRP, the better the ductility. Compared with the ductility of normal short LBL columns, when the cloth ratio was 1.2%, 1.8%, 2.3% and 2.9% respectively, the ductility of BFRP reinforced short LBL columns increased by 1.0%, 1.6%, 1.7% and 1.8% respectively.

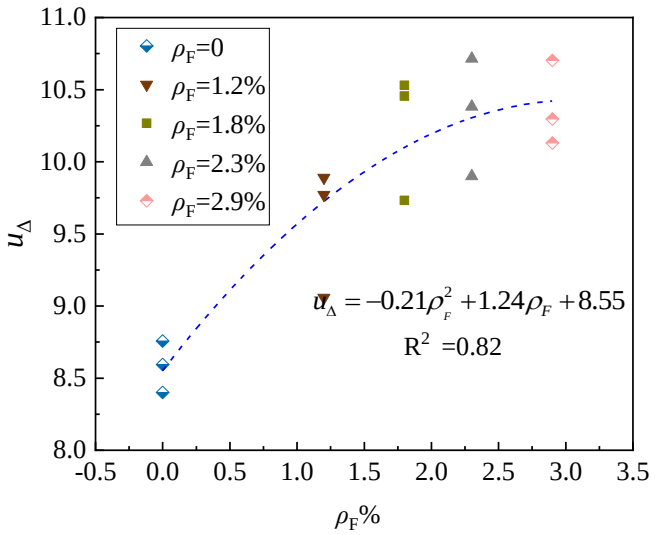

Fig. 9 Relationship between cloth ratio and ductility coefficient

3.5 Bearing capacity

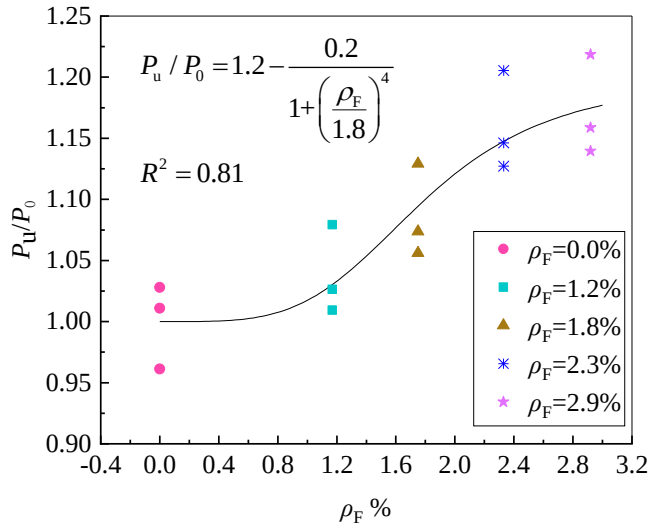

Fig. 10 Relationship between BFRP cloth ratio and ultimate load

The variation trend of the load-bearing capacity with different BFRP cloth ratio is shown in **Fig. 10**. The bearing capacity of the specimens increased with the increase of BFRP cloth ratio. As the increase of the equal difference of the cloth, the bearing capacity increased by 3.5%, 8.5%, 15.9%, and 17.0%, respectively. When the cloth ratio was less, the bearing capacity increased significantly. However, the improvement of bearing capacity was not obvious, when the cloth ratio increased from 2.3% to 2.9%. The

reasonable cloth ratio is 2.3%, which is four layers of BFRP. The relationship between the bearing capacity and cloth ratio of BFRP reinforced LBL can be expressed as follows:

$$P_u / P_0 = 1.2 - \frac{0.2}{1+\left(\frac{\rho_F}{1.8}\right)^4} \tag{5}$$

Where P_u is the bearing capacity of the columns; P_0 is the average bearing capacity of the normal short LBL columns.

It can be seen from the above analysis that the lateral restraint of BFRP increased the overall stiffness and ductility of the columns, enhanced the bearing capacity of the specimens.

4 Theoretical calculation model

4.1 Bearing capacity

4.1.1 Section shape

For FRP reinforced columns with circular cross-section, the lateral restraining force is uniformly distributed and has good restraining effect, while for FRP reinforced columns with square cross-section, the lateral restraining force is unevenly distributed [67]. The constraining effect is strongest near the column corners, and the constraint between the column corners is relatively weak. In the column corners, the BFRP cloth and the specimen cannot fit together well. In particular, the BFRP cloth will become harder after the glue is cured, so that the two cannot fit together well, so the constraint between the column corners is relatively weak. There are effective constraint regions and non-effective constraint regions [68]. The distribution of the non-effective constraint zone is a quadratic parabola, approximating the arc action mode, and the angle of the tangent at the end point is 45°, as shown in **Fig. 11**. We proposed the section shape coefficient k_s to calculate the ratio of the effective restraint area of the octagonal section to the total area, and the calculation formula is as follows.

$$A_i = \frac{4(b-2d)^2}{6} \times \tan 45° = \frac{2(b-2d)^2}{3} \tag{6}$$

$$A_e = b^2 - 2d^2 - \frac{2(b-2d)^2}{3} \tag{7}$$

$$k_s = \frac{A_e}{A_a} \tag{8}$$

Where A_a is the square cross-sectional area, A_i is the area of non-effective constraint area and A_e is the area of effective constraint area respectively; k_s is the cross-sectional shape coefficient; b is cross-sectional side length; d is chamfers side length .

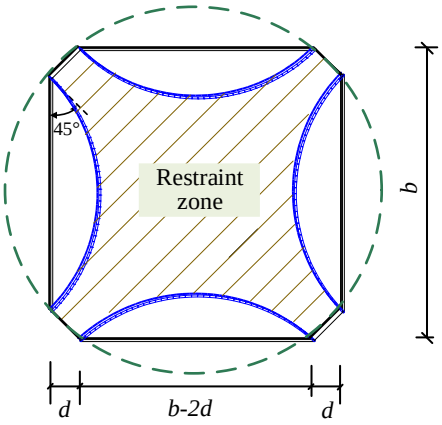

Fig. 11 Partition of equivalent restraint zone of square column

4.1.2 Lateral restraint strength and equivalent elastic modulus of BFRP

In the experimental study of FRP confined square columns, the FRP at the corner was usually torn first [69-70], and there was a great stress concentration in the FRP at the corner. The cross-sectional shape coefficient k_s is introduced for calculation to the lateral restraint strength f_l.

$$f_l = 2k_s \frac{E_{frp}\varepsilon_{frp}nt_f}{D} \tag{9}$$

Where E_{frp} is the elastic modulus of BFRP; ε_{frp} is the strain of BFRP at failure; D is the diameter of the equivalent circular cross-section; t_f is the thickness of BFRP, n is total layers of BFRP.

We proposed the calculation expression of the equivalent elastic modulus of BFRP along the fiber direction as follows:

$$G_l = 2k_s \frac{E_{frp}nt_f}{D} \tag{10}$$

4.1.3 Bearing capacity model

There were research results on the axial compression performance of FRP reinforced concrete rectangular columns, which had been incorporated into the design codes to serve as a reference for subsequent research and design. For the convenience of engineers, the strength of restrained columns was assumed to be linear with lateral restraint by FRP [71-73].

$$f_{cc} = f_{c0} + k_f f_l \tag{11}$$

Where f_{cc} is the peak stress of BFRP reinforced short LBL column; f_{c0} is the average compressive strength of normal short LBL column; k_f is the chamfer weakening coefficient.

The data of 15 specimens in this study were calculated and analyzed by linear regression, and the relationship between the peak stress of BFRP reinforced short LBL columns with square cross-section and the effective restraint stress of BFRP cloth was obtained. The fitting result is shown in **Fig. 12**. Therefore, the functional relationship between the peak stress of the BFRP reinforced specimens and the effective restraint

stress of BFRP cloth can be expressed as follows:

$$\frac{f_{cc}}{f_{c0}}-1=1.2\frac{f_l}{f_{c0}} \tag{12}$$

$$f_{cc}=f_{c0}+1.2f_l \tag{13}$$

Thus, the expression of axial compression bearing capacity N of BFRP reinforced LBL short columns is as follows:

$$N=f_{cc}A_a=\left(f_{c0}+1.2f_l\right)A_a \tag{14}$$

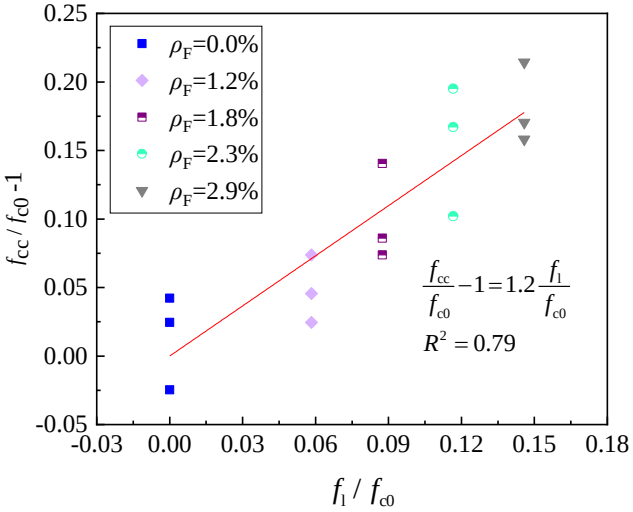

Fig. 12 Fitting result of confinement coefficient *k*

Table 3 Comparison of bearing capacity calculation values with test values

Specimens	σ_u (MPa)		Error (%)	P_u (kN)		Error (%)
	Calculated value	Test value		Calculated value	Test value	
SA300-1	54.7	54.7	0	536.1	536.1	0
SA300-1	58.5	58.5	0	573.3	573.3	0
SA300-1	57.5	57.5	0	563.8	563.8	0
S2B300-1	58.7	60.3	2.7	586.7	601.5	4.4
S2B300-2	62.5	58.7	6.5	624.4	586.9	4.4
S2B300-3	61.5	57.5	7.0	614.5	547.5	10.1
S3B300-1	60.7	64.1	5.3	609.0	627.8	5.3
S3B300-2	64.5	60.3	7.0	646.6	590.6	7.0
S3B300-3	63.5	61.0	4.1	636.7	597.8	4.1
S4B300-1	62.7	65.6	4.4	631.2	652.3	5.8
S4B300-2	66.5	61.9	7.4	668.9	618.4	5.4
S4B300-3	65.5	67.2	2.5	681.2	668.1	3.9
S5B300-1	64.7	68.3	5.3	653.4	671.4	5.6
S5B300-2	68.5	65.1	5.2	691.1	640.6	4.8
S5B300-3	67.5	66.4	1.6	681.2	647.7	2.1

To verify the correctness of the bearing capacity calculation method of BFRP

reinforced short LBL columns obtained by the theoretical formula, the calculated values are compared with the test values, as shown in Table 3. The calculated values of bearing capacity of the BFRP reinforced LBL columns agreed well with the test values. The results showed that the formula can effectively predict the bearing capacity of BFRP reinforced short LBL columns.

4.2 Stress-strain relationship

According to the stress-strain curve of BFRP reinforced short LBL columns drawn from the measured data (**Fig. 8**), the stress-strain model can be simplified into a three-stage model, namely elastic stage, elastic-plastic stage and plastic stage, as shown in **Fig. 13**. The model was based on several basic assumptions: (i) the LBL and BFRP are firmly bonded to form an integral forced component, and the load in the whole loading process is carried by the LBL and BFRP; (ii) at the yield point A(ε_y, σ_y), the slope of the second parabola is less than that of the first straight line; (iii) the parabola is smoothly connected with the third segment at the extreme point B(ε_p, σ_p); (iv) the end point of the third strain is the ultimate compressive strain.

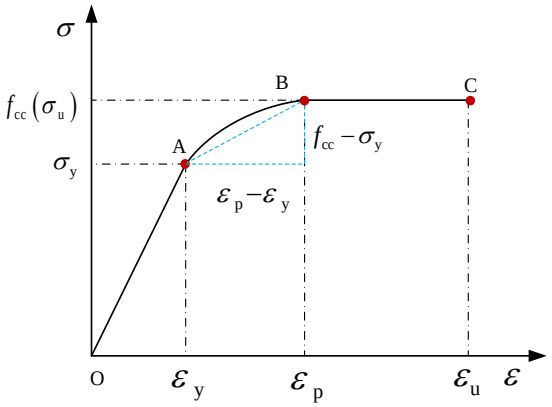

Fig. 13 Three stage stress-strain model

4.2.1 Elastic stage

In the elastic stage, the stress-strain relationship is positively proportional for BFRP reinforced short LBL columns. LBL and BFRP were well bonded to form an integral forced component, and the load was carried jointly by both.

The active confining pressure provided by BFRP increases the elastic modulus of the specimen and slightly increases the linear slope. The elastic modulus consists of two parts: the elastic modulus of the LBL itself and the equivalent elastic modulus of BFRP. The elastic modulus in the elastic stage can be expressed by the linear combination of the two:

$$E_{cc} = E_{c0} + k_E G_l \tag{15}$$

Where E_{cc} is the elastic modulus of columns; E_{c0} is the average elastic modulus of normal short LBL columns; k_E is the stress increase factor.

Based on the calculation and linear regression analysis of the relevant data (**Fig. 14**), the relationship between the elastic modulus of BFRP reinforced short LBL columns with

a square cross-section and the effective restraint stiffness of BFRP is obtained:

$$\frac{E_{cc}}{E_{c0}}-1=5.9\frac{G_l}{E_{c0}} \tag{16}$$

$$E_{cc}=E_{c0}+5.9G_l \tag{17}$$

Thus, the expression of stress-strain relationship of BFRP reinforced short LBL columns is as follows:

$$\sigma=E_{cc}\varepsilon=\left(E_{c0}+5.9G_l\right)\varepsilon \quad \left(\varepsilon\le\varepsilon_y\right) \tag{18}$$

The comparison between the elastic modulus calculation values and the test values are listed in **Table 4**.

Table 4 Comparison between calculation values of elastic modulus and test values

Specimens	The mean value of E_{cc}（MPa）		Error (%)
	Calculated value	Test value	
SA300	9258	9258	0
S2B300	10316	10202	1.1
S3B300	10845	10621	1.9
S4B300	11375	11130	2.1
S5B300	11903	12023	1.0

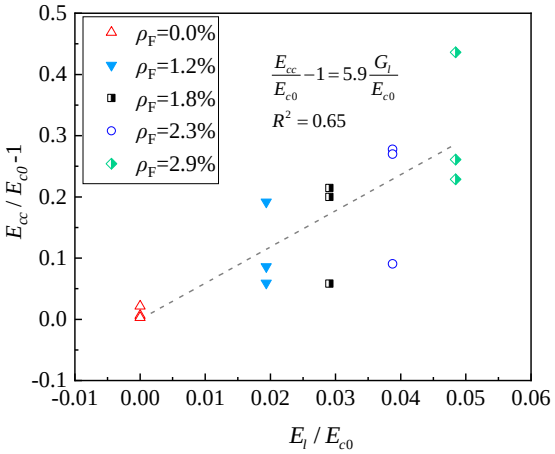

Fig. 14 Fitting result of stiffness increase factor k_E

4.2.2 Elastoplastic stage

The distribution of the stress-strain curve at this stage is similar a parabola (Fig. 8). Therefore, it is assumed that the expression of stress-strain relationship is:

$$\sigma=a\varepsilon^2+b\varepsilon+c \quad \left(\varepsilon_y<\varepsilon\le\varepsilon_p\right) \tag{19}$$

Where a, b and c are undetermined coefficients.

According to the relevant literature on the stress-strain relationship of FRP reinforced concrete column [74] and FRP reinforced wooden column [59], the strain value of the specimens was a displacement related quantity, which was related to the restraining strength. Through data analysis and fitting (**Fig. 15**), the strain expression of BFRP reinforced short LBL columns is obtained as follows:

$$\frac{\varepsilon_y}{\varepsilon_{c0}} = 1 - 2.1\frac{f_l}{f_{c0}} \tag{20}$$

$$\frac{\varepsilon_p}{\varepsilon_{c0}} = 1 + 19.2\frac{f_l}{f_{c0}} \tag{21}$$

Where ε_y is yield strain; ε_p is plastic strain; ε_{c0} is the average yield strain of normal short LBL columns.

The stress-strain curve passes through two points A and B and the slope at point B is zero. The expressions of undetermined coefficients *a*, *b* and *c* can be obtained from these three conditions:

$$a = -\left(f_{cc} - \sigma_y\right)/\left(\varepsilon_p - \varepsilon_y\right)^2 \tag{22}$$

$$b = 2\varepsilon_p\left(f_{cc} - \sigma_y\right)/\left(\varepsilon_p - \varepsilon_y\right)^2 \tag{23}$$

$$c = \sigma_y + \varepsilon_y^2\left(f_{cc} - \sigma_y\right)/\left(\varepsilon_p - \varepsilon_y\right)^2 - 2\varepsilon_y\varepsilon_p\left(f_{cc} - \sigma_y\right)/\left(\varepsilon_p - \varepsilon_y\right)^2 \tag{24}$$

Hence,

$$\sigma = \sigma_y - \frac{f_{cc} - \sigma_y}{\left(\varepsilon_p - \varepsilon_y\right)^2}\varepsilon^2 + \frac{2\varepsilon_p\left(f_{cc} - \sigma_y\right)}{\left(\varepsilon_p - \varepsilon_y\right)^2}\varepsilon + \frac{\varepsilon_y^2\left(f_{cc} - \sigma_y\right)}{\left(\varepsilon_p - \varepsilon_y\right)^2} - \frac{2\varepsilon_y\varepsilon_p\left(f_{cc} - \sigma_y\right)}{\left(\varepsilon_p - \varepsilon_y\right)^2} \quad \left(\varepsilon_y < \varepsilon \le \varepsilon_p\right) \tag{25}$$

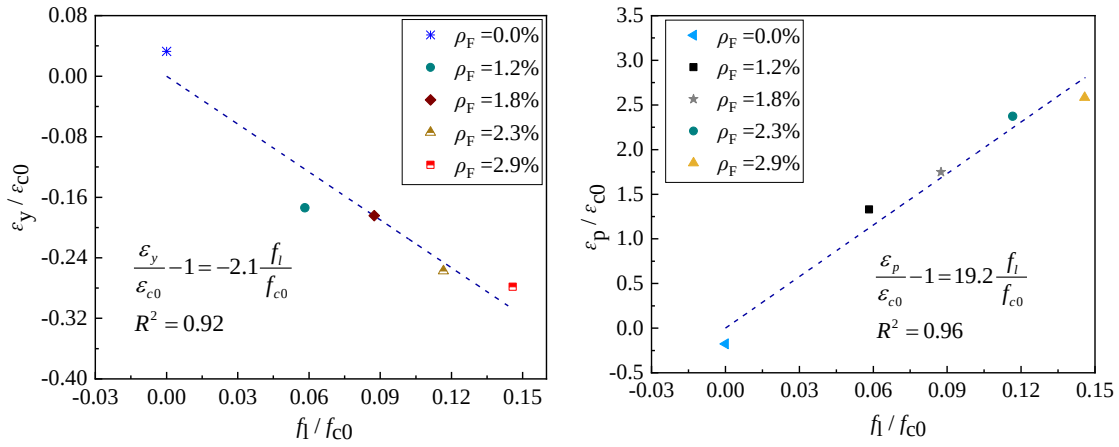

(a) Yield strain **(b) Plastic strain**

Fig. 15 Strain fitting coefficient

4.2.3 Plastic stage

In the plastic stage, the strain gauge pasted on the surface of BFRP cloth loses its function due to the breaking of BFRP cloth, and the real strain value after the breaking of BFRP cloth cannot be measured. In fact, the stress-strain distribution of BFRP reinforced short LBL columns had a long deformation platform. The stress-strain expression at this stage is:

$$\sigma = \sigma_u = f_{cc} = f_{c0} + 1.2 f_l \quad \left(\varepsilon_p < \varepsilon \le \varepsilon_u\right) \tag{26}$$

4.2.4 Stress-strain expression

Based on the above analysis, the three-stage stress-strain expression of BFRP reinforced short LBL columns is obtained:

$$\sigma=\begin{cases}\left(E_{c0}+5.9G_l\right)\varepsilon & \left(\varepsilon\le\varepsilon_y\right)\\ \sigma_y-\dfrac{f_{cc}-\sigma_y}{\left(\varepsilon_p-\varepsilon_y\right)^2}\varepsilon^2+\dfrac{2\varepsilon_p\left(f_{cc}-\sigma_y\right)}{\left(\varepsilon_p-\varepsilon_y\right)^2}\varepsilon+\dfrac{\varepsilon_y^2\left(f_{cc}-\sigma_y\right)}{\left(\varepsilon_p-\varepsilon_y\right)^2}-\dfrac{2\varepsilon_y\varepsilon_p\left(f_{cc}-\sigma_y\right)}{\left(\varepsilon_p-\varepsilon_y\right)^2} & \left(\varepsilon_y<\varepsilon\le\varepsilon_p\right)\\ f_{c0}+1.2f_l & \left(\varepsilon_p<\varepsilon\le\varepsilon_u\right)\end{cases} \tag{27}$$

The calculated values of stress-strain were compared with the test values. The values of SA300-3 and S4B300-2 were selected for comparative analysis and drawn in **Fig. 16**. It can be seen that the trend of change in the calculated value is consistent with the test value. This showed that the stress-strain model proposed in this study can accurately reflect the stress-strain relationship of BFRP reinforced short LBL columns.

Furthermore, the model proposed is used to calculate the stress-strain of AFRP and CFRP reinforced short LBL columns (**Fig. 17**). The comparison between calculation model and existing results shows that the calculation model proposed is accurate and universal.

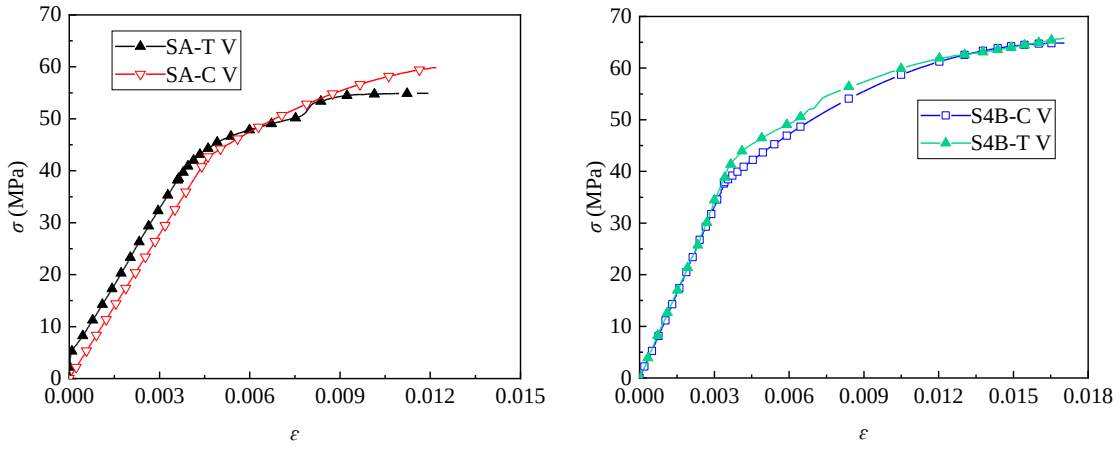

(a) ρ_F=0.0 **(b) ρ_F=2.3**

Fig. 16 Comparison between calculated values and test values of stress-strain curves (T V: test value, C V: Calculated value)

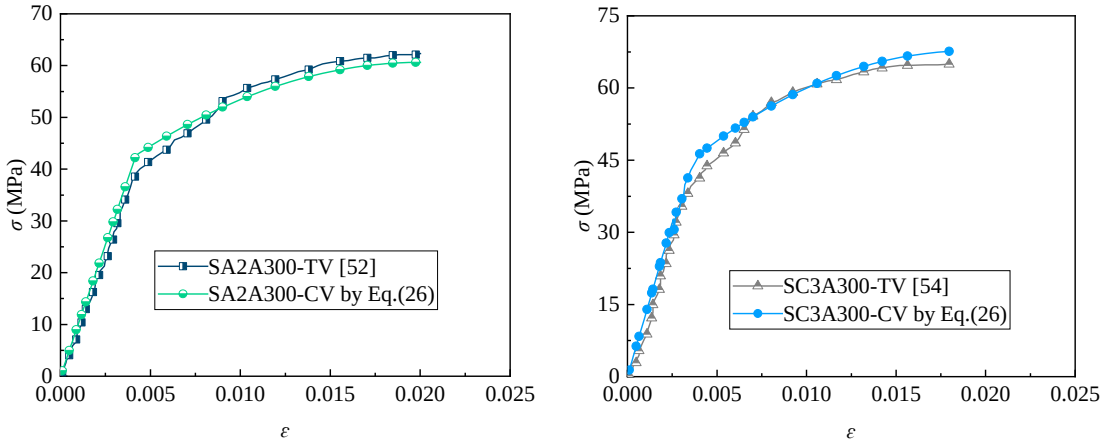

(a) AFRP reinforced short LBL column **(b) CFRP reinforced short LBL column**

Fig. 17 Comparison between calculation model and existing results of stress-strain curves

5 Conclusion

To investigate the effect of BFRP reinforced short LBL columns on axial compressive performance, a total number of 15 columns were conducted, including 12 BFRP reinforced short LBL columns (4 groups, 3 columns for each group, the cloth ratio is 1.2%, 1.8%, 2.3% and 2.9% respectively) and 3 normal short LBL columns, and tensile tests of 13 BFRP were carried out. The following conclusions can be drawn through the test results and analysis:

(1) The failure mode of BFRP reinforced short LBL columns and normal short LBL columns were buckling failure and adhesive layer failure. The average values of BFRP tensile strength and elastic modulus are 1488 MPa and 59.5 GPa respectively, and the average strain of BFRP at failure is 0.024.

(2) The BFRP reinforced short LBL columns showed better compressive ductility. Compared with the ductility of normal short LBL columns, when the cloth ratio is 1.2%, 1.8%, 2.3% and 2.9% respectively, the ductility of BFRP reinforced short LBL columns increased by 1.0%, 1.6%, 1.7% and 1.8% respectively.

(3) With the increase of BFRP cloth ratio, the compressive capacity of BFRP reinforced short LBL columns increased. Compared with the bearing capacity of normal short LBL columns, when the cloth ratio is 1.2%, 1.8%, 2.3% and 2.9% respectively, the bearing capacity of BFRP reinforced short LBL columns increased by 3.5%, 8.5%, 15.9% and 17.0% respectively. The most reasonable cloth ratio is 2.3%, which is four layers of BFRP. The calculation formula of compressive bearing capacity of BFRP reinforced short LBL columns was established.

(4) The obvious difference of stress-strain relationship between BFRP reinforced short LBL columns and normal short LBL columns was mainly reflected in the elastic-plastic stage. The larger the cloth ratio of BFRP was, the fuller the elastic-plastic stage was. The universal stress-strain model proposed can describe both the stress-strain relationship of FRP reinforced short LBL columns and normal short LBL columns.

Funding: This work was supported by the National Natural Science Foundation of China (No. 51878354 & 51308301); the Natural Science Foundation of Jiangsu Province (No. BK20181402 & BK20130978); Six talent peak high-level projects of Jiang-su Province (No. JZ-029); and Qinglan Project of Jiangsu Higher Education Institutions. Any research results expressed in this paper are those of the writer(s) and do not necessarily reflect the views of the foundations.

Acknowledgment: The writers gratefully acknowledge Ben Chen, Zhen Wang, Han Zhang, Ke Zhou, Xiaoyan Zheng, Shaoyun Zhu, Liqing Liu, Dunben Sun, Jing Cao, Yanjun Liu, Junhong Xu and others from the Nanjing Forestry University for helping.

The authors declare that they have no conflicts of interest to this work.

References

[1] Y. Huang, Y. Ji, W. Yu. Development of bamboo scrimber: A literature review. Journal of wood science 65(1) (2019): 1-10.

[2] L. Villegas, R. Moran, J.J. Garcia. Combined culm-slat Guadua bamboo trusses. Engineering Structures 184

(2019): 495-504.

[3] B. Li, J. Zhang, X. J. Zhou, et al. Effects on the protection of bamboo by cold plasma and 2D resin-based protective agent. Journal of Forestry Engineering 6(2) (2021): 57-63.

[4] J. Liu, A.P. Zhou, B.L. Sheng, et al. Effect of temperature on short-term compression creep property of bamboo scrimber. Journal of Forestry Engineering 6(2) (2021): 64-69.

[5] B. Sharma, A. van der Vegte. Engineered bamboo for structural applications. Nonconventional and Vernacular Construction Materials. Woodhead Publishing (2020):597-623.

[6] Liu Kewei, Durai Jayaraman, Shi Yongjiu, Kent Harries, Yang Jun, Jin Wei, Shi Yuechu, Wu Junqi, Pablo Jacome, David Trujillo. “Bamboo: A Very Sustainable Construction Material” - 2021 International Online Seminar summary report. Sustainable Structures 2(1) (2022): 000015.

[7] Y.J. Li, Z.C. LOU. Progress of bamboo flatten technology research. Journal of Forestry Engineering 6(4) (2021): 14-23.

[8] H.R. Liu, X.M. Yang, X.B. Zhang, et al. The tensile shear bonding property of flattened bamboo sheet. Journal of Forestry Engineering 6(1) (2021): 68-72.

[9] Leonel Mimendi, Rodolfo Lorenzo, Haitao Li. An innovative digital workflow to design, build and manage bamboo structures. Sustainable Structures 2(1) (2022): 000011.

[10] X. Sun, M.J. He, Z. Li. Novel engineered wood and bamboo composites for structural applications: State-of-art of manufacturing technology and mechanical performance evaluation. Construction and Building Materials 249 (2020): 118751.

[11] Y. Xiao, Z. Li., Y. Wu, et al. Research and engineering application progress of laminated bamboo structure. Building Structure 48(10) (2018): 84-88.

[12] H.T. Li , X.Y. Zheng , N. Guo, et al. Modern bamboo and timber structure. Beijing, China Building Industry Press, (2020): 257-262.

[13] D. Cheng, T Li, G.D. Smith, et al. The properties of Moso bamboo heat-treated with silicon oil. European Journal of Wood and Wood Products 76(4) (2018): 1273-1278.

[14] Y. Zhu, Q. Zhang, Q. Zeng. An optimizing study on the structure of bamboo laminate. Forestry and Grassland Machinery 27(2) (2016): 44-46.

[15] F. Xiao, Y. Q. Wu, Y.F. Zuo, et al. Preparation and bonding performance evaluation of bamboo veneer/foam aluminum composites. Journal of Forestry Engineering 6(3)(2021): 35-40.

[16] Z. Zhao, G. Yang, W. Fu, et al. Study on effect between anticorrosive deal method and mechanics performance of bamboo culm. Forestry and Grassland Machinery 27(4) (2016): 13-15+23.

[17] T. Reynolds, B. Sharma, K. Harries, et al. Dowelled structural connections in laminated bamboo and timber. Composites Part B: Engineering 90 (2016): 232-240.

[18] B. Sharma, A. Gatóo, M.H. Ramage. Effect of processing methods on the mechanical properties of engineered bamboo. Construction and Building Materials 83 (2015): 95-101.

[19] N.P.N. Pradhan, T.S. Paraskeva, and E.G. Dimitrakopoulos. Quasi-static reversed cyclic testing of multi-culm bamboo members with steel connectors. Journal of Building Engineering 27 (2020): 100983.

[20] A. Sinha, D. Way, S. Mlasko. Structural performance of glued laminated bamboo beams. Journal of Structural Engineering 140(1) (2014): 04013021.

[21] K.A. Harries, J. Bumstead, M. Richard, et al. Geometric and material effects on bamboo buckling behaviour. Proceedings of the Institution of Civil Engineers-Structures and Buildings 170(4) (2017): 236-249.

[22] C.S. Verma, V.M. Chariar. Stiffness and strength analysis of four layered laminate bamboo composite at macroscopic scale. Composites Part B: Engineering 45(1) (2013): 369-376.

[23] J.F. Correal, J.S. Echeverry, F. Ramírez, et al. Experimental evaluation of physical and mechanical properties of Glued Laminated Guadua angustifolia Kunth. Construction and Building Materials 73 (2014): 105-112.

[24] Y. Wei, K. Zhao, H. Chen, et al. Experimental study on the creep behavior of recombinant bamboo. Journal of Renewable Materials 8(3) (2020): 251.

[25] Y Zhong, H.Q. Ren, Z.H. Jiang. Effects of temperature on the compressive strength parallel to the grain of bamboo scrimbe. Materials 9(6) (2016): 436.

[26] G. Chen, H. Jiang, Y. Yu, et al. Experimental analysis of nailed LBL-to-LBL connections loaded parallel to grain. Materials and Structures 53(4) (2020): 1-13.

[27] Assima Dauletbek, Haitao Li, Zhenhua Xiong, Rodolfo Lorenzo. A review of mechanical behavior of structural laminated bamboo lumber. Sustainable Structures 1(1) (2021): 000004.

[28] L.M. Tian, Y.F. Kou, J.P. Hao. Axial compressive behaviour of sprayed composite mortar–original bamboo composite columns. Construction and Building Materials 215 (2019): 726-736.

[29] H.T. Li, Q.S. Zhang, G. Wu, et al. A review on development of laminated bamboo lumber. Journal of Forestry Engineering 1(6) (2016): 10-16.

[30] H.T. Li, G. Chen, Q.S. Zhang, et al. Mechanical properties of laminated bamboo lumber column under radial eccentric compression. Construction and building materials 121 (2016): 644-652.

[31] H.T. Li, G. Wu, Q.S. Zhang, et al. Mechanical evaluation for laminated bamboo lumber along two eccentric compression directions. Journal of wood science 62(6) (2016): 503-517.

[32] H.T. Li, R. Liu, R. Lorenzo, et al. Eccentric compression properties of laminated bamboo columns with different slenderness ratios. Proceedings of the Institution of Civil Engineers–Structures and Buildings 172(5) (2019): 315-326.

[33] J. Tao, L. Xie, J. Liu, et al. Research Progress of Structural Laminated Bamboo Lumber. China Forest Products Industry 57(12) (2020): 16-21.

[34] Jingwen Su, Haitao Li, Zhenhua Xiong, Rodolfo Lorenzo. Structural design and construction of an office building with laminated bamboo lumber. Sustainable Structures 1(2) (2021): 000010.

[35] Ruifeng Liang, Gangarao Hota. Development and evaluation of load-bearing fiber reinforced polymer composite panel systems with tongue and groove joints. Sustainable Structures 1(2) (2021): 000008.

[36] Xinmiao Meng, Daobo Zhang, Peng Feng, Nan Hu. Review on mechanical behavior of solar cells for building integrated photovoltaics. Sustainable Structures 1(2) (2021): 000009.

[37] A. Castelo, J.R. Correia, S. Cabral-Fonseca, et al. Inspection, diagnosis and rehabilitation system for all-fibre-reinforced polymer constructions. Construction and Building Materials 253 (2020): 119160.

[38] I. Basilio, R. Fedele, P.B. Lourenço, et al. Assessment of curved FRP-reinforced masonry prisms: experiments and modeling. Construction and Building Materials 51(2014): 492-505.

[39] V. Corinaldesi, G. Moriconi. Use of synthetic fibers in self-compacting lightweight aggregate concretes. Journal of building engineering 4 (2015): 247-254.

[40] Q.F. Lv, D. Yi, Y. Liu. Study of the bond behaviour between basalt fibre-reinforced polymer bar/sheet and bamboo engineering materials. Advances in Structural Engineering 22(14) (2019): 3121-3133.

[41] Y.L. Yu, Y. Huang, Y. Zhang, et al. The reinforcing mechanism of mechanical properties of bamboo fiber bundle-reinforced composites. Polymer Composites 40(4) (2019): 1463-1472.

[42] M. Mahdavi, P.L. Clouston, S.R. Arwade. A low-technology approach toward fabrication of laminated bamboo

lumber. Construction and Building Materials 29 (2012): 257-262.

[43] L.F. Zhang, W.Q. Liu, L. Wang, et al. Mechanical behavior and damage monitoring of pultruded wood-cored GFRP sandwich components. Composite Structure. 215 (2019) 502-520.

[44] H. Fang, B. Yu, W.Q. Liu, et al. Connections and structural applications of fibre reinforced polymer composites for civil infrastructure in aggressive environments. Composites Part B: Engineering 164 (2019) 129-143.

[45] E. Kandare, P. Luangtriratana, B.K. Kandola. Fire reaction properties of flax/epoxy laminates and their balsa-core sandwich composites with or without fire protection. Composites Part B: Engineering 56 (2014) 602-610.

[46] L Yang, X Li, H Fang, et al. Compressive behaviour of wood-filled GFRP square columns with lattice-web reinforcements. Construction and Building Materials 310 (2021): 125129.

[47] I.D.G.A. Subagia, Y. Kim, L.D. Tijing, et al. Effect of stacking sequence on the flexural properties of hybrid composites reinforced with carbon and basalt fibers. Composites Part B: Engineering 58 (214): 251-258.

[48] L.J. Ouyang, M.X. Chai, J. Song, et al. Repair of thermally damaged concrete cylinders with basalt fiber-reinforced polymer jackets. Journal of Building Engineering 44 (2021): 102673.

[49] X.B. Wu. Research Progress on Application of Basalt Fiber in Civil Engineering. Bulletin of the Chinese ceramic society 39(4) (2020): 1043-1049+1056.

[50] J Song, W.Y. Gao, L.J. Ouyang, et al. Compressive behavior of heat-damaged square concrete prisms confined with basalt fiber-reinforced polymer jackets. Engineering Structures 242 (2021): 112504.

[51] Y.J. Gao, Y. Zhou, J. Zhou, et al. Blast responses of one-way sea-sand seawater concrete slabs reinforced with BFRP bars. Construction and Building Materials 232 (2020): 117254.

[52] J. Feng, Y.Z. Zhou, P. Wang, et al. Experimental research on blast-resistance of one-way concrete slabs reinforced by BFRP bars under close-in explosion. Engineering Structures 150 (2017): 550-561.

[53] H. Najm, J. Secaras, P. Balaguru. Compression tests of circular timber column confined with carbon fibers using inorganic matrix. Journal of materials in civil engineering 19(2) (2007): 198-204.

[54] J.F. Dong, P. Jia, S.C. Yuan, et al. Compressive behaviours of square timber columns reinforced by partial wrapping of FRP sheets. Materials Research Innovations 19(sup1) (2015): S1-465-S1-468.

[55] Y Zhang, J Wang, J Lin, et al. Crushing mechanical responses of natural wood columns and wood-filled composite columns. Engineering Failure Analysis 124 (2021): 105358.

[56] R.B. O'Callaghan, D. Lacroix, K.E. Kim. Experimental investigation of the compressive behaviour of GFRP wrapped spruce-pine-fir square timber columns. Engineering Structures 252 (2022): 113618.

[57] Q.Y. Qiao, Z.Y. Yang, B. Mou. Experimental study on axial compressive behavior of CFRP confined square timber filled steel tube stub columns. Structures 24 (2020): 823-834.

[58] J.M Gattas., M.L. O'Dwyer, M.T. Heitzmann, et al. Folded hybrid FRP-timber sections: concept, geometric design and experimental behaviour. Thin-Walled Structures 122 (2018): 182-192.

[59] S.H. A, C.D. Zhou, L.G. Yang. Experimental investigation on axial compression behavior of timber columns strengthened with composite reinforcement method. China Civil Engineering Journal 54(2) (2021): 1-9.

[60] X. Wang, A. Zhou, L. Zhao, et al. Mechanical properties of wood columns with rectangular hollow cross section. Construction and Building Materials 214 (2019): 133-142.

[61] R.N. Emerson. In situ repair technique for decayed timber piles. Structures 2004: 1-9.

[62] R. Chidiaq. Axial compression of rounded wood poles reinforced with carbon fibers. New Jersey: State University; 2003.

[63] C.K. Hong, H.T. Li, D.Yang, et al. Compressive performance of AFRP reinforced laminated bamboo stub columns. Archives of Civil and Mechanical Engineering 22(1) (2022): 1-12.

[64] Z. Wang, H.T. Li, B. Fei, et al. Axial compressive performance of laminated bamboo column with aramid fiber reinforced polymer. Composite Structures 258 (2021): 113398.

[65] H. Li, H.T. Li, C.K. Hong, et al. Experimental investigation on axial compression behavior of laminated bamboo lumber short columns confined with CFRP. Composites Part A: Applied Science and Manufacturing 150 (2021): 106605.

[66] A.P.C. Duarte, B.A. Silva, N. Silvestre, et al. Experimental study on short rubberized concrete-filled steel tubes under cyclic loading. Composite Structures 136 (2016): 394-404.

[67] J.F. Jiang, P.D. Li, N. Nistico. Local and global prediction on stress-strain behavior of FRP-confined square concrete sections. Composite Structures 226 (2019): 111205.

[68] R. Abbasnia, H. Ziaadiny. Behavior of concrete prisms confined with FRP composites under axial cyclic compression. Engineering Structures 32(3) (2010): 648-655.

[69] J.J. Zeng, G. Lin, J.G. Teng, et al. Behavior of large-scale FRP-confined rectangular RC columns under axial compression. Engineering Structures 174 (2018): 629-645.

[70] D. Mostofinejad, E. Ilia, N. Mortazavi. Fibre-reinforced polymer efficiency in square columns with different corner radii. Proceedings of the Institution of Civil Engineers-Structures and Buildings 171(3) (2018): 241-252.

[71] J.W. Park, Y. K. Hong, G.S. Hong, et al. Design formulas of concrete filled circular steel tubes reinforced by carbon fiber reinforced plastic sheets. Procedia engineering 14 (2011): 2916-2922.

[72] ACI Committee. ACI 440.2 R-08: Guide for the Design and Construction of Externally Bonded FRP System for Strengthening Concrete Structures. USA: Farmington Hills (2008):76.

[73] Canadian Standards Association. CAN/CSA S6-06: Canadian Highway Bridge Design Code. Toronto, Ontaria, Canada: CSA (2014).

[74] Y.R. Zhang, Y. Wei, J. Bai , et al. Stress-strain model of an FRP-confined concrete filled steel tube under axial compression. Thin-Walled Structures 142 (2019): 149-159.